*Progress In Electromagnetics Research C, Vol. 81, 101–113, 2018*

# A Comparative Study of Quasi-FEA Technique on Iron Losses Prediction for Permanent Magnet Synchronous Machines

**Pedram Asef[1, 2], Roman Bargallo Perpina[1], M. R. Barzegaran[2, *], Jianning Dong[3], Andrew Lapthorn[4], and Osama A. Mohammed[5]**

**Abstract**—The paper presents an advanced quasi-FEA technique on the iron losses prediction using Bertotti's iron loss separation models, in which a curve fitting is taken into account for coefficients calculation of each model. Moreover, the skin effect and saturation consideration are applied in order to check the accuracy through the relative error distribution in the frequency domain of each model from low up to high frequencies 50 to 700 (Hz). Additionally, this comparative study presents a torque-speed-flux density computation that is discussed and presented. The iron loss characteristics of a radial flux permanent magnet synchronous machine (PMSM) with closed-slots and outer rotor topology are also discussed. The quasi-finite-element (FE) analysis was performed using a 2-D and 3-D FEA, where the employed quasi-2-D FEA is proposed and compared with 3-D FEA, and along with experimental verifications. Finally, all the iron-loss models under realistic and non-ideal magnetization conditions are verified experimentally on a surface-mounted PMSG for wind generation application.

## 1. INTRODUCTION

Wind power generation and development have been increasing during the past two decades worldwide [1], in which permanent magnet synchronous machines (PMSM)s are employed for their high energy production and efficiency in both geared-drive and direct-drive configurations [2–6]. However, achieving higher performance from conventional PMSMs requires notable attention into the design principles of electrical machines. The iron loss calculation itself takes a considerable share in the design process, where a number of considerations must be taken into account. The skin effect consideration for an accurate eddy-current loss calculation via 3-D modeling has been lately addressed [7–9] and has significantly developed the understanding of eddy-current behavior. Moreover, the use of the physical segmentation technique on the construction is another recent achievement in suppressing eddy-currents (particularly in the PMs); however, that comes always with a high manufacturing cost [10].

Steentjes et al. [11] present an accurate prediction of iron losses in soft magnetic materials for various frequencies and magnetic flux densities that is important for an enhanced design of electrical machines. The IEM-Formula, which is used in this literature, resolves the limitation of the common iron-loss models by introducing a high order term of the magnetic flux density. Furthermore, the IEM-Formula was extended in order to include the influence of higher order harmonics and minor loops. In another paper, Eggers et al. [12] describe IEM-Formula with semi-physically based parameters for non-linear material behavior in electrical machines. However, both studies focused on simulation without experimental tests.

*Received 27 October 2017, Accepted 10 January 2018, Scheduled 12 February 2018*
* Corresponding author: M. R. Barzegaran (barzegaran@lamar.edu).
[1] Department of Electrical Engineering, Polytechnic University of Catalonia-Barcelona Tech, Barcelona, Spain. [2] Department of Electrical Engineering, Lamar University, Beaumont, USA. [3] Department of Electrical Engineering, TU Delft, Delft, the Netherlands. [4] Department of Electrical Engineering, University of Canterbury, Christchurch, New Zealand. [5] Department of Electrical Engineering, Florida International University, Miami, USA.

The modeling of the iron losses based on Bertotti's approach has been classically studied in many references such as [13–15] via FEA. The models can be either carried out at the post-processing or nonlinear resolution stage in an electrical machine in order to increase the efficiency through an advanced estimation of iron losses distribution in the model.

Fratila et al. show two iron loss models, based on Bertotti's decomposition method using FEA accounting for the eddy-currents in the damper bars of a turbo-generator. Moreover, the used methods have been validated experimentally for no-load condition [16].

Rasilo et al. investigated on the losses in the laminated core of a 150-kVA wound-field synchronous machine with calorimetric measurements and a numerical iron-loss model for steel laminations. The effect of rotor lamination material on total core losses has been studied through measuring and simulating the machine with three prototype rotors [17]. In another valuable work, a comparison of frequency and time domain iron and magnet loss has been presented, where the focus is on recognizing the significance of including the analysis of higher harmonics in the electromagnetic loss calculation [18].

Pfingsten et al. [19] studied the global operating point dependent losses using a local transient loss formulation. In this work, the time and spatial distributions of flux density and the effect of choosing the best operating point have been included.

This paper deals with the impact of a segmentation consideration on each machine's part for a detailed predication of iron loss distribution in the model, in which the technique allows designers to provide an advanced iron loss estimation via a 2-D model. We develop an original quasi-FEA method for the calculation of the iron losses. The proposed technique is based on a harmonic of the radial and tangential components of flux density at each part. For this reason, Bertotti's iron loss separation models [13, 20–25] with two terms, three terms, and variable coefficient approaches have been applied to iron losses modeling, in which the multi-generalized reduced gradient nonlinear (M-RGN) method [26] was used for determining the best fitted coefficients. The iron loss models account for the skin effect

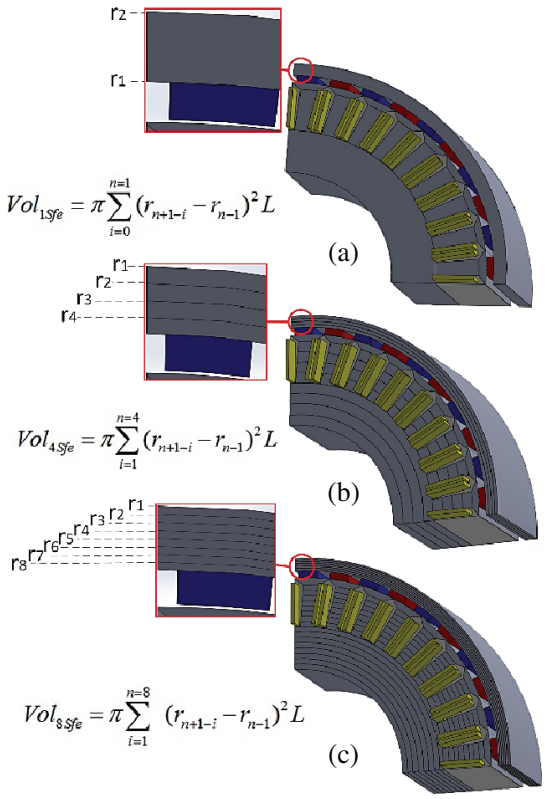


**Figure 1.** 3D segmented FEM model of the 36/40 PM synchronous machine, (a) 1-segmented, (b) 4-segmented, and (c) 8-segmented.

as well as saturation considerations, where the flux density components have been calculated using 2-D FEA and verified by 3D-FEA.

An advanced analysis from 50 to 700 (Hz) was performed to provide existing harmonics and the radial/tangential components of the flux density at each machine's part, where each part has been theoretically segmented into four and eight segments for a more improved iron loss calculation on the PMSM.

## 2. PROPOSED IRON LOSS MODELING

The iron loss modeling development will introduce a quasi-FEA technique based on a theoretical segmentation in frequency domain, in which iron losses are evaluated locally, in each space point of the iron. Therefore, the eddy-current loss reduction is not aimed through segmentation in this paper, although theoretical segmentation allows the design procedure to provide a detailed iron loss calculation at each machine's part using 2D-FEA for the advanced iron losses distribution.

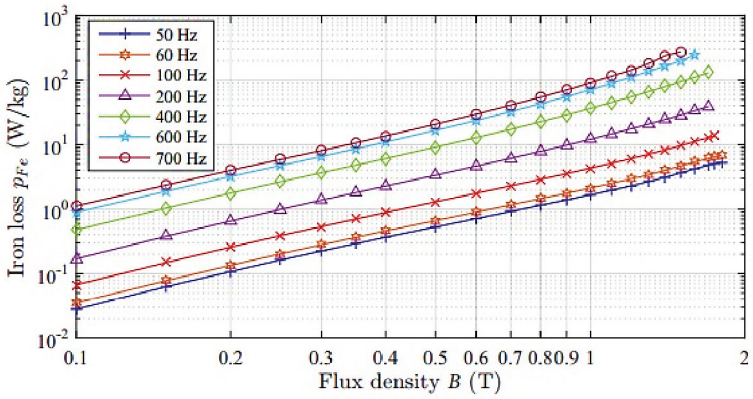


**Figure 2.** Iron loss results obtained from Epstein test.

The proposed technique deals with the geometry, in which flux density calculation at each part (rotor yoke, tooth top, tooth, and stator yoke) will be subdivided into three types, 1, 4, and 8-segmented models (shown in Figure 1). The eight-segmented model has the highest number of segments as limitation at each part due to mesh sizing. Accordingly, the volume calculation at each iron part for each model is:

$$\begin{aligned} Vol_{1Sfe} &= \pi \sum_{i=0}^{n=1} (r_{n+1-i} - r_{n-1})^2 L \\ Vol_{4Sfe} &= \pi \sum_{i=1}^{n=4} (r_{n+1-i} - r_{n-1})^2 L \\ Vol_{8Sfe} &= \pi \sum_{i=1}^{n=8} (r_{n+1-i} - r_{n-1})^2 L \end{aligned} \tag{1}$$

where $r_{n+1-i}$ is the outer radius of the segment, $r_{n-1}$ the inner radius of each iron segment, and $L$ the axial length of the machine which is 100 (mm). Thus, the volume of each segment is $\pi(r_{n+1-i} - r_{n-1})2 \cdot L$, in which $n$ is the number of segments: The effect of the calculated volume is shown in 3D segmented FEM model in Figures 1(a)–(c).

### 2.1. Frequency Domain Computation

The most commonly used approach for iron loss calculation in electrical machines is decomposing the flux density waveform obtained from finite element models (FEM) into frequency components, then

applying the Bertotti model to each component. Mathematically, the approach is described as:

$$W_{fe} = \sum_{1}^{n_{\max}} p_{fe,n}(B_n, nf_1) \tag{2}$$

where $B_n$ is the amplitude of $n$th harmonic component of flux density, $f_1$ the fundamental frequency, and $p_{fe,n}$ the iron loss of the $n$th harmonic calculated using Equation (3). Usually, the calculation is carried out during the post-processing of FEM, and the flux density is decomposed into the radial component $B_{rn}$ and tangential component $B_{tn}$ further, which is:

$$W_{fe} = \sum_{1}^{n_{\max}} p_{fe,r,n}(B_{rn}, nf_1) + \sum_{1}^{n_{\max}} p_{fe,t,n}(B_{tn}, nf_1) \tag{3}$$

This proposed quasi-FEA technique is evaluated using accurate loss separation and identification of loss coefficients in the presence of skin effect at an Epstein frame (illustrated in Figure 2, with respect to the IEC 60404-2 standard). Based on empirical approach [25], the iron loss ($P_{fe}$) is separated into a hysteresis component ($P_h$), an eddy current component ($P_e$), an anomalous model ($P_a$), and saturation term ($P_{sat}$) [13]. Under sinusoidal alternating excitation, they are calculated for each iron segment as:

$$P_{fe} = P_h + P_e + P_a + P_{sat.} = k_h f \widehat{B}^{\alpha} + k_e f^2 \widehat{B}^{\beta} + k_a f^{1.5} \widehat{B}^{\gamma} + k_e k_{s1} \widehat{B}^{k_{s2}} f^2 + k_e \hat{B}^{k_{sat}+2} f^2 \tag{4}$$

$k_h$, $k_e$, $k_a$, $\alpha$, $\beta$, and $\gamma$ are loss coefficients, in which M-RGN approach will be carried out to calculate the best fitted values. $B$ is the peak value of the flux density in each segment.

For an engineering approach, the effect of excess loss is combined with the eddy current loss to form a total eddy current loss. Therefore, iron loss is calculated by the three terms equation as:

$$P_{fe} = k_h f \widehat{B}^{\alpha} + k_e f^2 \widehat{B}^{\beta} + k_e k_{s1} \widehat{B}^{k_{s2}} f^2 \tag{5}$$

The eddy currents in the motor core are strongly influenced by the skin effect phenomena, especially under high excitation frequencies. The eddy current term can be improved as in the following equation to take skin effect into account [20]:

$$P_e = k_e \left( \frac{\sinh(d\sqrt{f}) - \sin(d\sqrt{f})}{\cosh(d\sqrt{f}) - \cos(d\sqrt{f})} \right) f^{1.5} \widehat{B}^{\beta} \tag{6}$$

where $d$ is another loss coefficient which depends on the steel sheet thickness.

It is well known that loss coefficients $k_h$, $\alpha$ and $k_e$ exhibit a significant variation with flux density $B$ and frequency $f$, as opposed to the conventional model [21]. Various models with variable coefficients have been proposed in literature to improve the accuracy in wide frequency and flux density ranges [22, 23]. In this paper, the following model is used to take into account both the skin effect and the loss coefficient variation:

$$P_{fe} = k_h(f, \hat{B}) f \hat{B}^{h(\hat{B})} + k_e \left( \frac{\sinh(d\sqrt{f} - \sin(d\sqrt{f})}{\cosh(d\sqrt{f}) - \cos(d\sqrt{f})} \right) f^{1.5} \hat{B}^{\beta} + k_e k_{s1} \hat{B}^{k_{s2}+2} f^2 + k_e \hat{B}^{k_{sat}+2} f^2 \tag{7}$$

where $k_h$, $f$, $B$, $h(B)$, $k_{s1}$, $k_{s2}$, $k_{sat}$ and $k_e B$ are polynomials in $f$ and $B$, and the formats of these functions differ between Eqs. (5) and (6) as given:

$$\begin{aligned}
k_h(f, \hat{B}) &= k_{h0} + k_{h1} f + k_{h2} f^2 + k_{h3} \hat{B} \\
h(\hat{B}) &= h_0 + h_1 \hat{B} \\
k_e(\hat{B}) &= k_{e0} + k_{e1} \hat{B} + k_{e2} \hat{B}^2 + k_{e3} \hat{B}^3 \\
k_{s1}(f, \hat{B}) &= k_{s10} + k_{s11} f + k_{s12} f^2 + k_{s13} \hat{B} \\
k_{s2}(f, \hat{B}) &= k_{s20} + k_{s21} f + k_{s22} f^2 + k_{s23} \hat{B} \\
k_{sat}(f, \hat{B}) &= k_{sat0} + k_{sat1} f + k_{sat2} f^2 + k_{sat3} \hat{B}
\end{aligned} \tag{8}$$

The total iron losses for each segment using Equations (1) and (5) can be defined for 1, 4, and 8-segmented models as follows:

$$\begin{aligned} P_{fe1S,total} &= Vol_{1sfe} \cdot P_{fe} \\ P_{fe4S,total} &= Vol_{4sfe} \sum_{i=1}^{n=4} P_{fe(n+1-i)} \\ P_{fe8S,total} &= Vol_{8sfe} \sum_{i=1}^{n=8} P_{fe(n+1-i)} \end{aligned} \tag{9}$$

## 2.2. Coefficient Identification

Loss coefficients in Equations (2) and (6) are normally obtained from the measured loss data using curve fitting, in which the M-RGN was carried out to determine the best values with the lowest error. Iron losses of M400-50A iron sheet (with nonlinear $BH$ curve) samples under various flux densities and frequencies measured from Epstein test are shown in Figure 2. Equations (2), (3) and (5) are used for curve fittings. The three equations are referred as the three term model, two term model and variable coefficient model below. All the curve fittings are completed with sufficiently small residual, i.e., $r_2 > 0.999$. Table 1 shows the obtained coefficients.

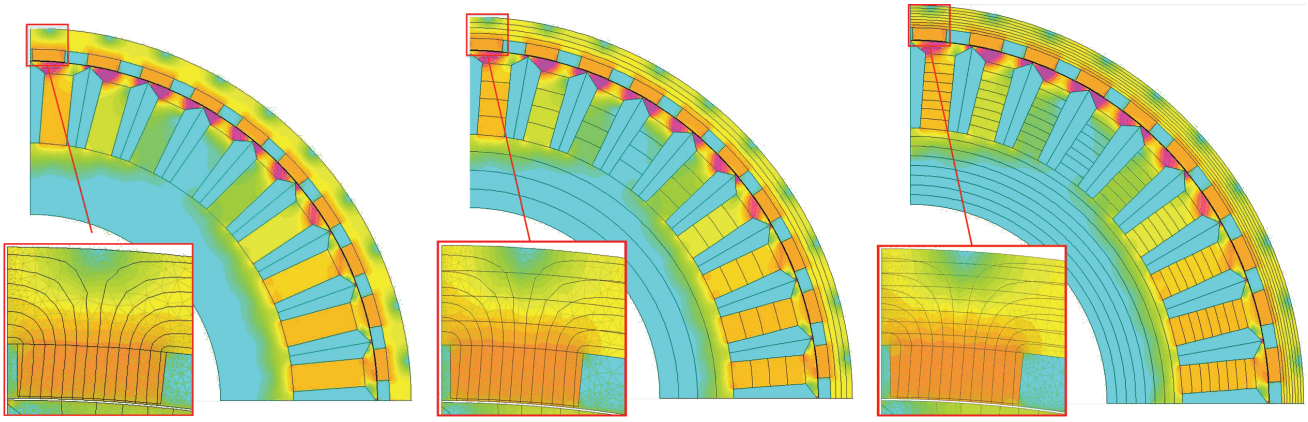


**Figure 3.** 2D flux density distribution on (a) 1-segmented, (b) 4-segmented, and (c) 8-segmented FE models.

## 3. EVALUATION OF THE PROPOSED QUASI-FE MODEL

The 2-D FE models are calculated based on the proposed quasi-FE technique using Equations (7)–(9) for each iron segment, where Equation (1) is defined. The flux density distribution, as a significant variable of the study, is calculated through FEM for different numbers of axial segments in Figure 3. The preferred 2-D FE is only due to the number of nodes which is 31258, whose gains much be less time-consuming simulation. The boundary setup used for each model considers each segment not physically separated. Thus, the purpose of theoretical segmentation is to provide a distinct average value at each segment block. Iron losses are calculated at the measured flux density and frequency points using the obtained loss coefficients and three iron loss models, respectively. Relative error distributions of the three models are compared with measured experimental data for different frequencies shown in Figure 4 based on Equations (2) and (3). Table 1 shows the obtained coefficients. All the three models predict the iron losses with high accuracy under high flux densities and frequencies. However, both the three term model and two term model result in significantly high errors under relatively low flux densities. Unsurprisingly, the best fit is achieved by the variable coefficient model, except for several points at

very low flux density (0.1 T), and the relative errors are ±10%. The calculated results from the variable coefficient model and measured data at no load condition are compared in Figure 5, in which good curve fitting between calculated and measurement results exists based on material properties of steel M-19 fully-processed non-oriented silicon with 0.36 mm and 29 gauge, where a higher frequency causes a larger iron loss.

The saturation loss calculation in the laminated stator and rotor cores are predicted via the local waveforms of the magnetic flux densities in Equation (4). Single-valued magnetization curves are used to consider saturation effects originating from the nonlinear material behavior. The magnetic material is utilized up to 2.1 T in the considered machine. Second-order effects, originating from hysteresis

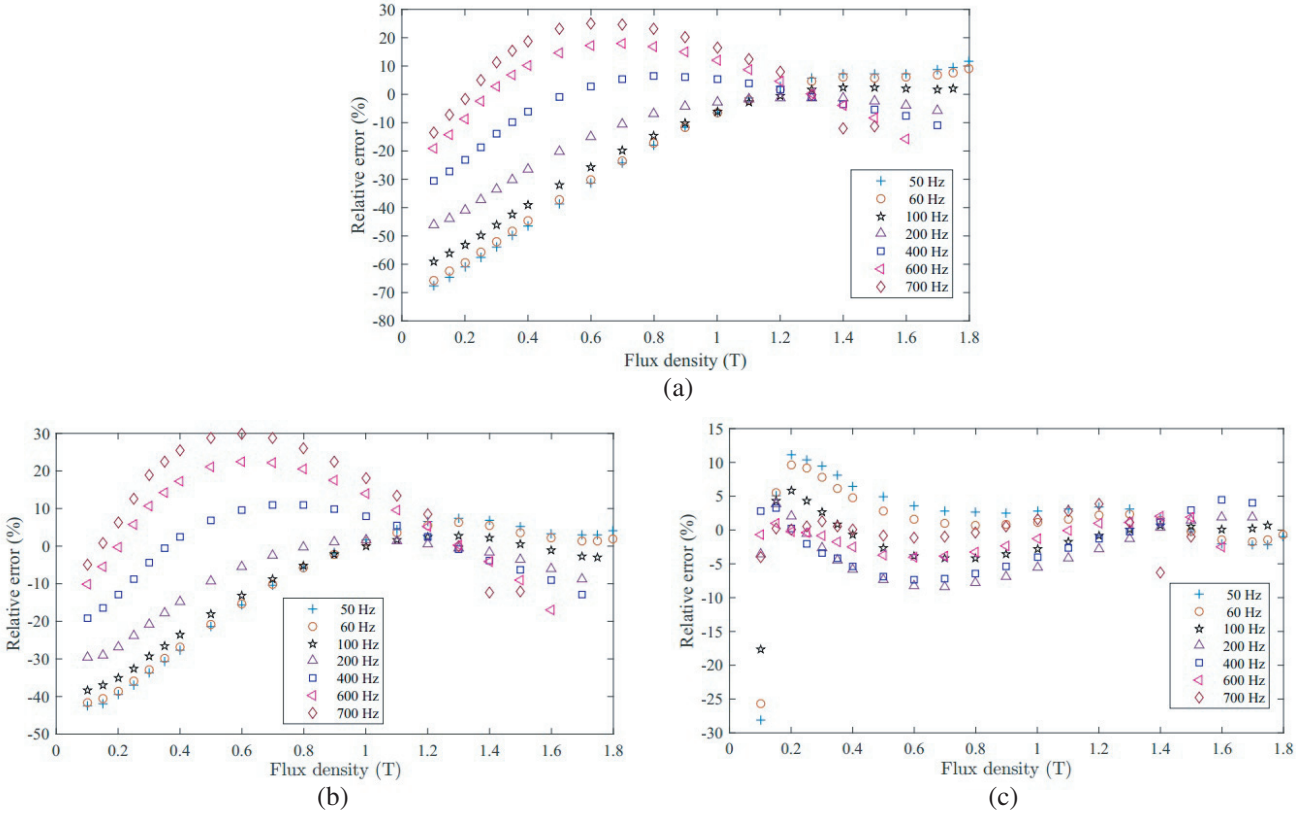


**Figure 4.** Relative error distributions of the three iron loss models: (a) three term model (b) two term model (c) variable coefficient model.

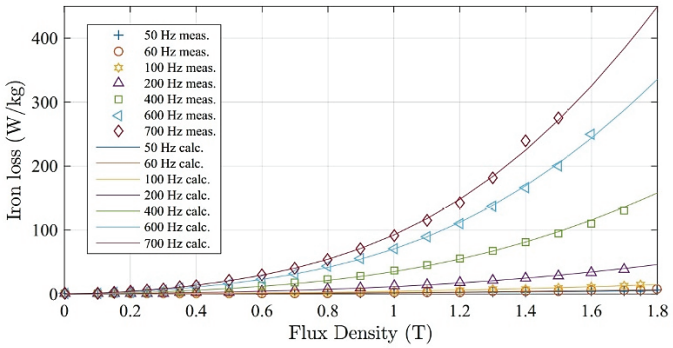


**Figure 5.** Comparison between calculated results of the variable coefficient model and measured ones at a standard frame.

**Table 1.** Loss coefficients obtained from curve fitting.

| Coefficient | Three term model | Two term model | Variable coefficient model |
|---|---|---|---|
| $h$ | 2.386 | 2.03 | NaN |
| $k_h$ | 0.02193 | 0.02193 | NaN |
| $k_e$ | $1.845 \times 10^{-4}$ | $1.845 \times 10^{-4}$ | NaN |
| $k_a$ | $3.152 \times 10^{-9}$ | NaN | NaN |
| $k_{s1}$ | $25.7 \times 10^{-7}$ | $25.12 \times 10^{-7}$ | $26.2 \times 10^{-7}$ |
| $k_{s2}$ | 3.6543 | 3.2313 | 3.9872 |
| $h_0$ | NaN | NaN | 0.2936 |
| $h_1$ | NaN | NaN | 0.07778 |
| $k_{h0}$ | NaN | NaN | $-0.002409$ |
| $k_{h1}$ | NaN | NaN | $4.253 \times 10^{-6}$ |
| $h_{h3}$ | NaN | NaN | 0.02895 |
| $d$ | NaN | NaN | 0.01826 |
| $k_{e0}$ | NaN | NaN | 0.02093 |
| $k_{e1}$ | NaN | NaN | $-0.01927$ |
| $k_{sat}$ | $1.043 \times 10^{-8}$ | $1.001 \times 10^{-8}$ | $1.361 \times 10^{-9}$ |

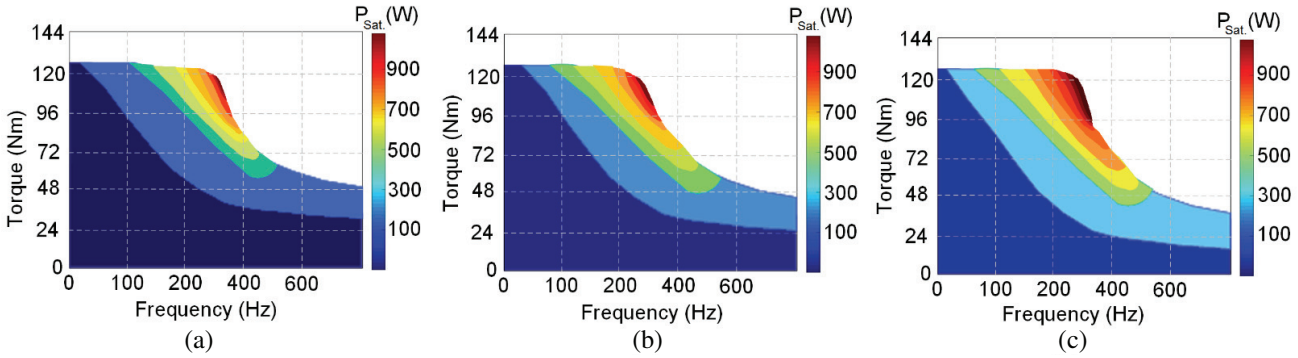


**Figure 6.** The torque-frequency-saturation loss presentation through the last term of Equation (5) for, (a) the FE one-segmented, (b) FE four-segmented, and (c) eight-segmented techniques.

behavior, are neglected. The saturation term is specifically at the area around the transition point at high torques and high speeds with a large proportion.

The nonlinear (saturation) loss without segmentation consideration is shown as smaller area of significant loss value of 900 (W) in Figure 6(a). However, through the four-segmented FE model, a slightly larger amount of saturation loss can be reported which is obviously presented via the color bar with a larger critical area by 950 (W) seen in Figure 6(b). The eight-segmented FE model has a larger area of critical loss which is clearly represented in Figure 6(c). The quasi-FEA technique is limited to the eight-segmented blocks due to mesh's size, where a single complete triangle mesh is required at each block.

The total iron loss calculation with skin effect consideration for stator and rotor cores is successfully done through Equation (10) and based on the proposed quasi-FEA technique (in Figure 7), in which a larger amount of iron losses at low and high frequencies can be seen via aid of a color bar at the four- and eight-segmented models that are illustrated in Figures 7(a) and 7(b), respectively. The proposed eight-segmented model using the quasi-FEA technique has estimated a larger significant iron losses, in which Figure 7 presents the peak total iron loss for maximum torque of 122 (N.m), at 400 (Hz) by

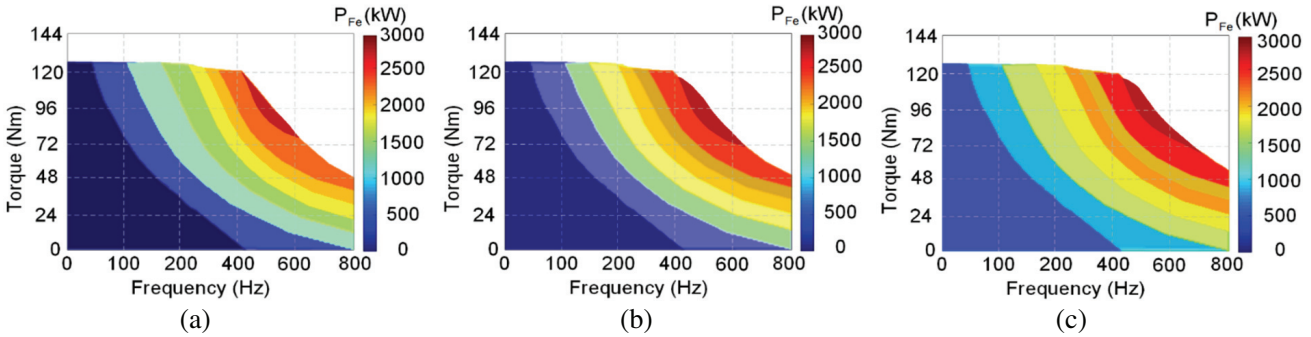


**Figure 7.** Total predicted iron losses using variable coefficient model as function of torque and frequency, where (a) the typical 2-D FE iron loss modeling, (b) the quasi-2-D-FE technique with four-segmented observation, and (c) the proposed quasi-2-D-FE technique with eight-segmented observation.

2.01, 2.55, and 2.78 (kW) for conventional, four-segmented quasi-FEA, and proposed eight-segmented quasi-FEA technique, respectively. The proposed eight-segmented quasi-FEA model predicts with a larger area of significant losses than the conventional (Figure 7(a)) and four-segmented techniques due to a better mesh which is comparable to 3-D FEA.

Accurate calculation of the field harmonics at each single area (more specific by segmentation) of the iron parts is the main contribution of the work using a proposed quasi-FE technique. For example, through segmenting one tooth into eight, the tooth-top area is presented with much higher harmonics and related loss, whereas only considering the absolute value of a full tooth shows lesser filed harmonics in the critical areas. Additionally, the proposed model (in Figure 7(c)) illustrates a higher amount of iron loss at low frequencies between 0 and 350 (Hz). Moreover, the quality of constancy in torque between 0 and 400 (Hz) is a perfect match with the goal of the machine's operation.

## 4. 3D FEA AND EXPERIMENTAL VERIFICATIONS

After analyzing the PMSM machine based on the proposed quasi-FEA technique, in which a 2-D FEA is used, the 3-D FEA is investigated along with experimental verification. The Bertotti's iron loss separation models are employed to a PMSM with a permanently deliverable torque of 60 (Nm). The cross section of the laminated stator and rotor core of the twenty pole-pair PMSM under study is shown in Figures 1 and 8. The maximum rotational speed of the machine is 2400 (rpm). A double-layer fractional-slot winding is used to generate the airgap electromagnetic field. The rotor of the investigated machine is excited through buried magnets.

The proposed quasi-FE technique using 2-D FE model is verified with a 3-D FE model, in which the mesh is generated with a high quality with 544289 elements, 163013 nodes as shown in Figure 8, and its 3-D FE magnetic flux density distribution (as shown in Figure 9). The experimental setup is

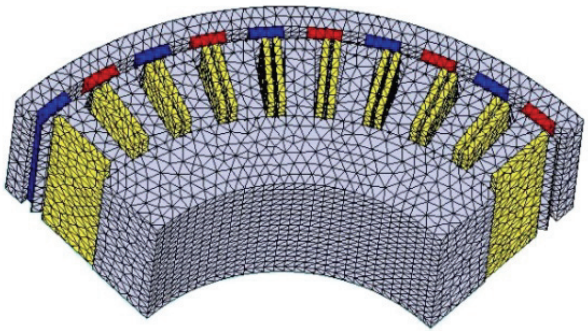

**Figure 8.** 3D mesh generation.

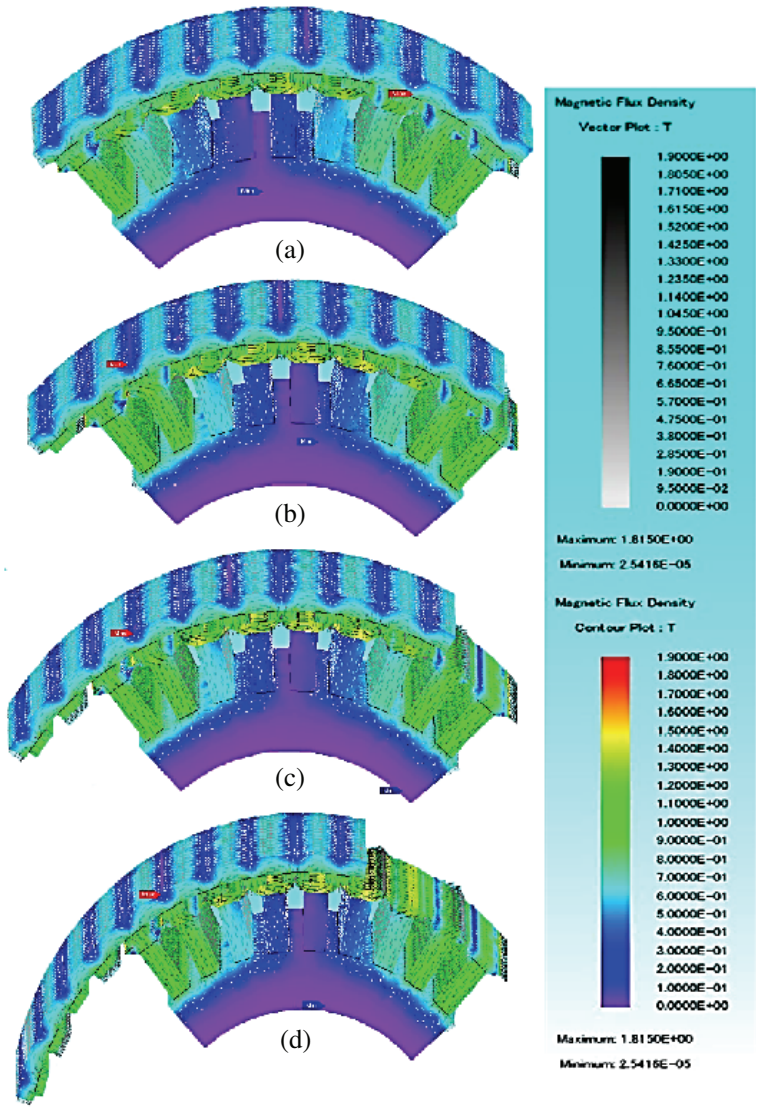


**Figure 9.** 3D mesh generation.

presented in Figure 12. The proposed technique results in a faster and cheaper simulation analysis than the 3-D FEA and has comparable accuracy. The stored airgap flux density through the proposed quasi-FEA technique is verified by the 3-D FEA and also experimental data (test), in which a good agreement can be seen between them in Figure 10.

Field harmonic verification for various orders from fundamental to 15th order at each iron part is illustrated in Figure 11. Using a typical technique, the magnetic field density and its corresponding harmonics are calculated for each iron part (rotor and stator yokes), whereas those data are calculated for smaller segments (4 or 8 times smaller) and considerably higher number of mesh elements and nodes by the proposed eight-segmented quasi-FEA technique. Regarding the proposed technique, the field harmonics calculated based on both the conventional models and the proposed model are employed to predict the iron loss on eight measured data points, and compared with the 3-D FEA and experiment results, the FEA results are calculated under sinusoidal three-phase current excitation. The developed test bench is shown in Figure 12 with, in the foreground, the 5.5 kW, twenty pole-pairs, synchronous generator that is the subject of this study. The generator is coupled to an asynchronous machine employed to drive it at different speeds. Moreover, the studied generator was instrumented with several magnetic flux sensors at each segment in order to compare the measured waveforms with the simulated

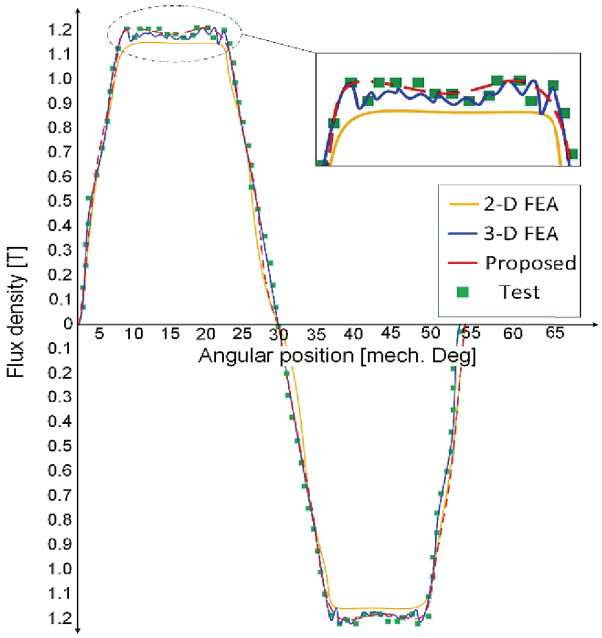


**Figure 10.** Airgap flux density verification.

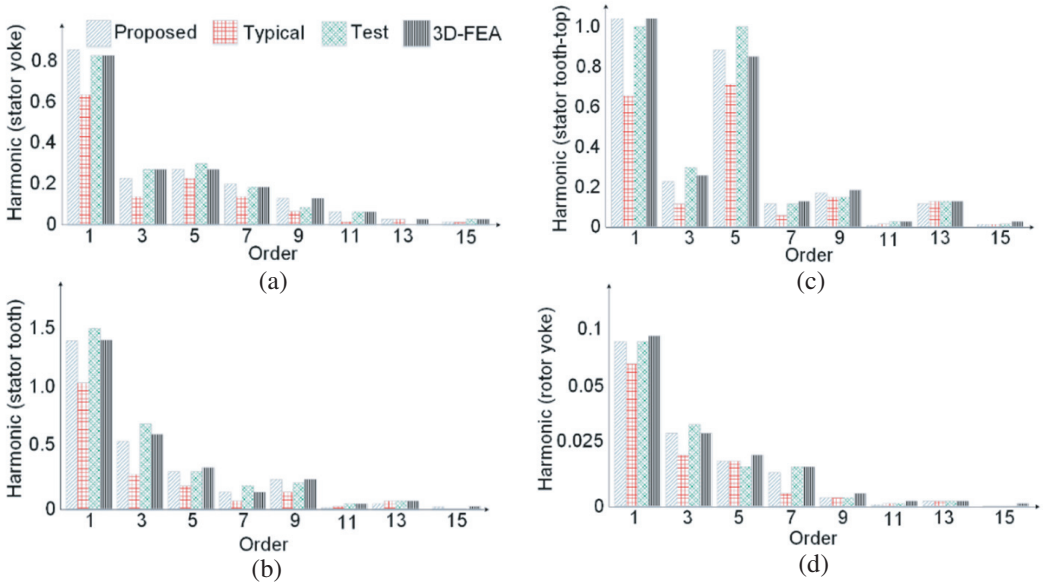


**Figure 11.** Comparison of field harmonics in iron parts of the machine at (a) stator yoke, (b) stator tooth, (c) stator tooth-top, and (d) rotor yoke.

ones [24]. The iron loss is determined by the tests with the sinusoidal and PWM supplies and also performed with the rotor in a standstill condition. All the stator and rotor iron losses are measured, and besides, the technique can be applied. Consider all the iron loss active in only iron parts of the PMSM in order to remove certain uncertainties in the iron-loss measurement. This method allows the use of (the international standards, such as the IEEE 112 method B) with a good accuracy [25].

As Figure 12(a) illustrates that the comparison of iron loss obtained via eight-segmented technique presents a good agreement with the 3-D FEA and experiment results. The error between the proposed model and experiment results is due to neglecting the current harmonic, slot opening effect and fringing

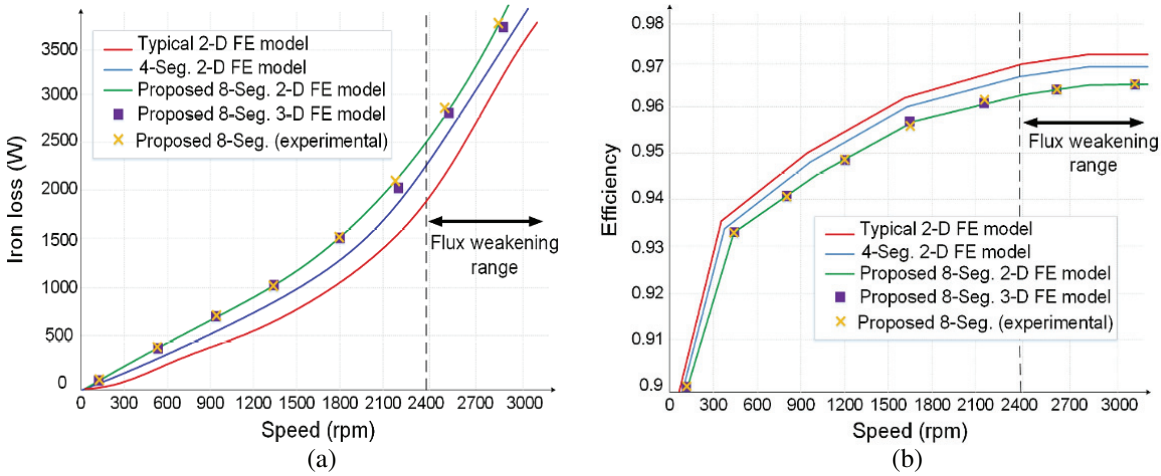


**Figure 12.** Comparison of the electromagnetic-based objectives for a wide speed operation, in which (a) shows iron loss trend, and (b) affected machines' efficiency because of losses computation.

effect. On the contrary, the iron loss predicted by the conventional model is obviously underestimated. Under flux weakening, the difference between the conventional model and the other two FE models (four- and eight-segmented) quickly increases as speed increases.

Figure 12(b) presents the comparison of PMSM efficiency obtained via the proposed method. The PMSM efficiency of the proposed method is acceptable compared with the experimentally measured machine efficiency and FEA results. The PMSM efficiency computed using the proposed method is slightly higher than experiment results, mainly due to neglecting the phase current harmonic. It should be mentioned that only one FE model is built, while both levels of the proposed technique are used to predict the most accurate and fastest way to achieve the objectives of the study. Moreover, a significant increase of iron loss in the flux weakening range, particularly in the range after passing via the transition point, is evident.

## 5. CONCLUSION

Iron losses prediction for the radial flux PMSMs may be a critical design aspect, in which a highly precise estimation using 3-D FEA is normally very time consuming and brings additional cost into the design process. We believe that new techniques that challenge these two drawbacks are very useful to machine design. Quasi-FEA techniques might decrease the accuracy of the results due to simplifications occasionally. However, the proposed 2-D quasi-FEA technique presented in this paper demonstrates acceptable precision. An advanced and verified analytical methodology which is based on Bertotti's iron loss separation models in frequency domain with eddy-currents and saturation considerations is employed to calculate iron losses for each segment separately. The proposed 2-D quasi-FEA technique with variable coefficient model of iron losses is sufficiently passed the 3-D FEA and experimental verifications. With respect to the order, the proposed eight- and four-segmented approaches are more accurate models than the experimental findings with less than 1% error, respectively. The proposed technique can be useful for the rapid design of PMSM with advanced prediction.

## REFERENCES

1. Asef, P., "Design, characteristic analysis of PM wind generator based on SMC material for small direct-drive wind energy conversion system," *International Conference on Renewable Energy Research and Application (ICRERA)*, 41, DOI: 10.1109/ICRERA.2014.7016437, USA, 2014.
2. Harrison, R., E. Hau, and H. Snel, *Large Wind Turbines Design and Economics*, Wiley, New York, 2000 (ISBN 0471-494569).

3. Dubois, M. R., "Optimized permanent magnet generator topologies for direct-drive wind tur-bines," Ph.D. dissertation, Delft Univ. Technol., Delft, The Netherlands, 2004.
4. Grauers, A., "Design of direct-driven permanent-magnet generators for wind turbines," Ph.D. dissertation, Chalmers Univ. Technol., Goteborg, Sweden, 1996.
5. Poore, R. and T. Lettenmaier, "Alternative design study report: Wind PACT advanced wind tur-bine drive train designs study," *NREL, Golden, CO*, Rep. NREL/SR-500-33196, Aug. 2003.
6. Cotrell, J. R., "A preliminary evaluation of a multiple-generator drive train configuration for wind turbines," presented at *the 2002 ASME Wind Energy Symp., 40th AIAA Aerosp. Sci. Meeting Exhibit*, Collection Tech. Papers, Reno, NV, Jan. 14–17, 2002.
7. Martin, F., et al., "Improved analytical determination of eddy current losses in surface mounted permanent magnets of synchronous machine," *IEEE Trans. Magn.*, Vol. 50, No. 6, 1–8, Jun. 2014.
8. Hemeida, A., et al., "Comparison of methods for permanent magnet eddy-current loss computations with and without reaction field considerations in axial flux PMSM," *IEEE Trans. Magn.*, Vol. 51, No. 9, 1–8, Sep. 2015.
9. Kakhki, M. T., et al., "New approach for accurate prediction of eddy current losses in laminated material in the presence of skin effect with 2-D FEA," *IEEE Trans. Magn.*, Vol. 52, No. 3, 1–4, Mar. 2016.
10. Huang, W. Y., et al., "Optimization of magnet segmentation for reduction of eddy-current losses in permanent magnet synchronous machine," *IEEE Trans. Energy Conv.*, Vol. 25, No. 2, 381–386, 2010.
11. Steentjes, S., et al., "Iron-loss model with consideration of minor loops applied to FE-simulations of electrical machines," *IEEE Trans. Magn.*, Vol. 49, No. 7, 3945–3948, Jul. 2013.
12. Eggers, D., et al., "Advanced iron-loss estimation for nonlinear material behavior," *IEEE Trans. Magn.*, Vol. 48, No. 11, 3021–3024, Nov. 2012.
13. Bertotti, G., "General properties of power losses in soft ferromagnetic materials," *IEEE Trans. Magn.*, Vol. 24, No. 1, Jan., 1988.
14. Bertotti, G. and M. Pasquale "Physical interpretation of induction and frequency dependence of power losses in soft magnetic materials," *IEEE Trans. Magn.*, Vol. 28, No. 5, Sep. 1992.
15. Bertotti, G., et al., "An improved estimation of iron losses in rotating electrical machineS," *IEEE Trans. Magn.*, Vol. 27, No. 6, Nov. 1991.
16. Fratila, M., et al., "Iron loss calculation in a synchronous generator using finite element analysis," *IEEE Tran. Energy Conv.*, Vol. PP, No. 99, 1–8, doi: 10.1109/TEC.2017.2648512, 2017.
17. Rasilo, P., et al., "Experimental determination and numerical evaluation of core losses in a 150-kVA wound-field synchronous machine," *IET Electric Power App.*, Vol. 7, No. 2, 97–105, doi: 10.1049/iet-epa.2012.02422013.
18. Kowal, D., et al., "Comparison of frequency and time-domain iron and magnet loss modeling including PWM harmonics in a PMSG for a wind energy application," *IEEE Trans. Energy Conversion*, Vol. 30, No. 2, 476–486, 2015.
19. Pfingsten, G. V., et al., "Operating point resolved loss calculation approach in saturated induction machines," *IEEE Trans. Ind. Electr.*, Vol. 64, No. 3, 2538–2546, 2017.
20. Boglietti, A., A. Cavagnino, M. Lazzari, and M. Pastorelli, "Predicting iron losses in soft mag-netic materials with arbitrary voltage supply: An engineering approach," *IEEE Trans. Magn.*, Vol. 39, No. 2, 981–989, 2003.
21. Krings, A. and J. Soulard, "Overview and comparison of iron loss models for electrical ma-chines," *Journal of Electrical Engineering*, Vol. 10, No. 3, 162–169, 2010.
22. Ionel, D. M., M. Popescu, S. J. Dellinger, T. J. E. Miller, R. J. Heideman, and M. I. McGilp, "On the variation with flux and frequency of the core loss coefficients in electrical machines," *IEEE Trans. Ind. Appl.*, Vol. 42, No. 3, 658–667, May 2006.
23. Ionel, D. M., M. Popescu, M. I. McGilp, T. J. E. Miller, S. J. Dellinger, and R. J. Heideman, "Computation of core losses in electrical machines using improved models for laminated steel," *IEEE Trans. Ind. Appl.*, Vol. 43, No. 6, 1554–1564, Nov. 2007.

24. Huang, Y., J. Dong, J. G. Zhu, and Y. Guo, "Core loss modeling for permanent-magnet motor based on flux variation locus and finite-element method," *IEEE Trans. Magn.*, Vol. 48, No. 2, 1023–1026, 2012.
25. Gerlando, A. D. and R. Perini, "Evaluation of the effects of the voltage harmonics on the extra iron losses in the inverter fed electromagnetic devices," *IEEE Trans. on Energy Conv.*, Vol. 14, No. 1, 57–62, Mar. 1999.
26. Lasdon, L. S., et al., "Design and testing of a generalized reduced gradient code for nonlinear optimization," *Case Western Reserve University, National Technical Information Service U.S. Department of Commerce (NTIS)*, AD-A009-402, 1–45, Mar. 1975.